AIAA JOURNAL
Vol. 37, No. 6, June 1999

Density Matrix and Rate Equation Analyses for Picosecond Pump/Probe Combustion Diagnostics

Thomas Settersten* and Mark Linne†
Colorado School of Mines, Golden, Colorado 80401-1887
James Gord‡
U.S. Air Force Research Laboratory, Wright–Patterson Air Force Base, Ohio 45433-7103
and
Gregory Fiechtner§
Innovative Scientific Solutions, Inc., Dayton, Ohio 45440-3638

Further developments in picosecond pump/probe combustion diagnostics are described. The rate equation formalism originally used to model the pump/probe interaction is not entirely appropriate for a 2-ps interaction. For that reason, a new nonperturbative density matrix model that more exactly describes the pump/probe interaction is presented. Our goal is to discover how well the pump/probe interaction is described by the rate equations, when the interaction occurs within the rate equation limits, or to find a similarly simple expression. The model is described, results are presented, and then a comparison between the two formalisms is made.

Nomenclature

A_{21}	= Einstein coefficient for spontaneous emission, s^{-1}
D	= sample volume focal diameter, m
$E(z, t)$	= electric field, V/m
$\boldsymbol{E}(z, t)$	= electric field vector, V/m
$\hat{\boldsymbol{e}}_z$	= unit vector in the z direction
f^L	= laser repetition rate, s^{-1}
$f(u)\,\mathrm{d}u$	= fraction of atoms in the velocity interval $[u, u + \mathrm{d}u]$
g_i	= degeneracy of level where i is 1 or 2
i	= $\sqrt{-1}$
k_B	= Boltzmann constant, J/K
k_0	= optical wave propagation constant, m^{-1}
l	= beam interaction length, m
m	= mass of atom, kg
N_{tot}	= total number density of absorbing species, m^{-3}
$P_{\mathrm{av}}^{\mathrm{pump}}$	= average power of the pump beam, W
$P(z, t)$	= material polarization, C m^{-2}
$\boldsymbol{P}(z, t)$	= material polarization vector, C m^{-2}
$\tilde{p}(z, t)$	= complex polarization envelope function, C m^{-2}
T	= translational temperature, K
t	= time, s
u	= atomic velocity component along the optical axis $\hat{\boldsymbol{e}}_z$, m/s
V	= volume, m^3
$\boldsymbol{V}$	= interaction Hamiltonian, J
V_{21}, V_{12}	= off-diagonal elements of the interaction Hamiltonian, J
z	= spatial coordinate along the beam path, m
α_{mod}	= pump/probe modulation depth
Γ_{21}	= combined spontaneous emission and collisional de-excitation rates, s^{-1}
γ_{21}	= collisional dephasing rate, s^{-1}
$\Delta\nu_{1/2}^L$	= laser bandwidth, s^{-1}
Δz	= difference in pump and probe path lengths, m
ε^R, ε^I	= real and imaginary parts of the complex electric field envelope function, V/m
$\varepsilon(z, t)$	= electric field envelope, V/m
$\tilde{\varepsilon}(z, t)$	= complex electric field envelope function, V/m
ε_0	= permittivity of free space, F/m
μ_{12}, μ_{21}	= dipole matrix elements, C m
$\langle\mu\rangle$	= expectation value for the dipole moment, C m
ν_{12}	= transition frequency, s^{-1}
ρ	= density matrix
ρ_{11}, ρ_{22}	= diagonal density matrix elements; probabilities that the atom is in state 1 or 2
ρ_{21}, ρ_{12}	= off-diagonal density matrix elements; coherences between states 1 and 2
$\tilde{\sigma}_{21}$	= complex envelope function for the coherence
σ_{21}^R, σ_{21}^I	= real and imaginary parts of the envelope function for the coherence
τ	= retarded time, s
$\varphi(z, t)$	= slowly varying optical phase term
ω_0	= angular frequency of optical wave, s^{-1}
ω_{12}	= transition angular frequency, s^{-1}
*	= complex conjugate

Introduction

DURING the past 20 years, laser diagnostics have provided critical experimental data on species number density, temperature, and velocity in combustion flowfields. As discussed in detail by Eckbreth,[1] these techniques provide information that cannot be acquired using more conventional means. Each laser diagnostic technique can be applied only within limited conditions, however, and numerous tradeoffs are involved. Examples include a reduction in sensitivity in trade for spatial resolution; a requirement for corrections, calibrations, and simplified models in trade for low detection limits; an elimination of spatial resolution in trade for an absolute measurement, free from calibrations, corrections, or simplifications; and so on. Unfortunately, not all of the operating conditions of interest to practical combustion are addressed by the current techniques. Therefore, we are developing an entirely new combustion diagnostic, pump/probe spectroscopy, which has specific attributes not currently available to combustion researchers. These include 1) absolute determination of number density, without calibrations or corrections; 2) excellent spatial resolution; 3) insensitivity to the collisional environment, a diagnostic that works well at high pressures; and 4) a high-speed technique capable of detecting turbulent fluctuations and rapid transients. As with other diagnostics, we have traded away attributes, i.e., low detection limits, to achieve these.

Presented as Paper 98-0306 at the AIAA 36th Aerospace Sciences Meeting, Reno, NV, Jan. 12–15, 1998; received March 17, 1998; revision received Sept. 10, 1998; accepted for publication Sept. 14, 1998. Copyright © 1998 by the American Institute of Aeronautics and Astronautics, Inc. All rights reserved.

*Graduate Research Assistant, Center for Combustion and Environmental Research.
†Associate Professor, Center for Combustion and Environmental Research. Member AIAA.
‡Senior Research Chemist, Propulsion Directorate. Member AIAA.
§Research Scientist. Member AIAA.

Much of our research, therefore, focuses on mitigation of limitations to the pump/probe technique.

In the past, we have demonstrated that picosecond pump/probe spectroscopy provides an absolute determination of number density, without calibrations or corrections.[2] It is, essentially, a spatially resolved absorption measurement. Even molecules with poor fluorescence yield can be detected with pump/probe spectroscopy. Our estimates of species detection limits[3] indicate that the technique will prove useful for combustion research. In Ref. 3, for example, we predict a detection limit for CH around 10^{12} cm^{-3} for the conditions specified in that paper. We expect that pump/probe measurements will be insensitive to the collisional environment as well because it is possible to make the measurement over timescales much smaller than normal collisional times, and the transform-limited bandwidth of a picosecond pulse is significantly broader than single linewidths. Pressure effects on linewidth, therefore, should not propagate to the signal. With respect to measurement speed, an easily explained tradeoff between sensitivity and speed can provide measurement bandwidths between 500 Hz and 41 MHz (Ref. 3).

Our goal here is to take this diagnostic one step further, by subjecting the original rate equation expressions for pump/probe spectroscopy[4] to rigorous examination, using a quantum mechanically correct formalism. This is done to discover how well the pump/probe interaction is described by the rate equations (when the interaction occurs within the rate equation limits) or to find a similarly simple expression. In what follows we briefly describe the pump/probe technique and the rate equation results. We then present the density matrix formalism and our numerical approach. Next the behavior of a single propagating pulse is described and then is compared to rate equation results both within and outside the rate equation limits. Finally, the density matrix prediction of pump/probe modulation is compared to the rate equation prediction, exhibiting very good agreement within the rate equation limits.

Pump/Probe Spectroscopy

In pump/probe spectroscopy, the output from a continuous wave (cw) mode-locked laser is tuned to a transition of interest, and the beam is split into two portions. The pump beam is directed through a modulator and is crossed with the probe beam in the flame. This beam crossing forms a sample volume within the flame (Fig. 1). The pump modulation is impressed upon the resonant molecules in the sample volume because the populations of the ground and excited state are modified by the presence of the pump beam. These populations then modulate the probe beam at the intersection via absorption and stimulated emission, changing the probe irradiance at the modulation rate. This change in irradiance is defined as the modulation depth, expressed as a fraction of the total probe irradiance. After the flame, the pump beam reaches a beam stop, and the probe beam is detected. The detector signal is then synchronously demodulated using a lock-in amplifier. The measured probe modulation depth is proportional to the concentration of molecules. For optically thin conditions, the modulation depth will be at most a few percent. Nevertheless, for mode-locked lasers,[5] the minimum detectable modulation depth is approximately 10^{-8}.

We currently use a Spectra-Physics regeneratively mode-locked Ti:sapphire laser, equipped with both 2- and 60-ps optics. This laser produces about 1.8 W of output when pumped with 8 W from an intracavity-doubled, diode-pumped Nd:YVO_4 laser, with autocorrelation pulse widths around 1.4 ps in the 2-ps configuration. The transform-limited bandwidth is about 0.4 nm.

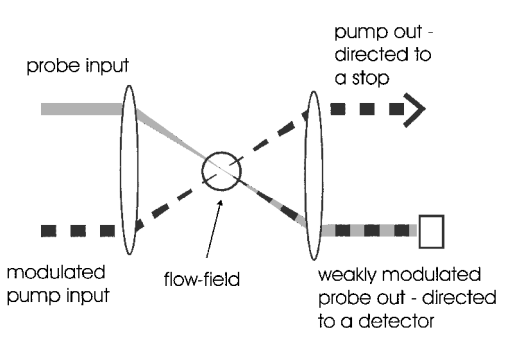

Fig. 1 Schematic of single-point pump/probe interaction in the flowfield.

In our experiments, both the pump and probe are in resonance with the same transition. For a two-level atom, the rate equations then give a modulation depth described by[4]

$$\alpha_{\mathrm{mod}} = \left[ln\left(\frac{1}{\sqrt{2}-1}\right)\right]^2 \frac{c^4 P_{\mathrm{av}}^{\mathrm{pump}} N_{\mathrm{tot}} l}{16\pi^3 D^2 h f^L \left(\Delta\nu_{\frac{1}{2}}^L\right)^2} \times \left[\frac{A_{21}^2}{\nu_{12}^5}\frac{g_2}{g_1}\left(1+\frac{g_2}{g_1}\right)\right] \quad (1)$$

The modulation resides on a large carrier (typically 10^4–10^7 larger than the modulated portion of the signal). Detecting this small signal is straightforward, and the demodulated signal is related directly to the number density of absorbers. The other terms in Eq. (1) are usually known or can be measured. We demonstrated that pump/probe absorption spectroscopy provides an absolute determination of number density when this equation was applied to our potassium measurements and then compared to atomic absorption spectroscopy using a tungsten filament lamp.[2]

The model given in Eq. (1) assumes an optically thin analyte, the linear absorption regime, a two-level system, a temporal top-hat pulse profile, and a broad laser bandwidth with respect to the absorption linewidth. The optically thin analyte assumption then leads to an assumption that the pump pulse is not absorbed as it passes through the medium, leading to an excited state population that does not change with position. The probe pulse is assumed to stimulate both absorption and emission, whereas the pump pulse stimulates absorption without stimulating emission. Finally, quenching is assumed negligible.

The rate-equation-based pump/probe model has recently been extended[3] for a molecular pump/probe interaction by accounting for numerous ro/vibrational levels, including the individual Boltzmann fractions, Einstein rate constants for each line, and the overlap between the laser linewidth and the individual lines pumped by the laser. It was simply assumed that the interaction could be represented by a summation over a number of distinct two-level resonances. Further details are provided in Ref. 3.

Density Matrix Model

As stated in the Introduction, we expect that pump/probe measurements will be insensitive to the collisional environment because it is possible to make the measurement in timescales much shorter than normal collisional times. Our pulsewidths are typically 2 ps long, and the probe pulse is adjusted to trail the pump pulse by only a few pulsewidths. These time frames are significantly shorter than the collision times, coherence lifetimes, and excited-state lifetimes of molecules in atmospheric pressure flames. This necessarily means that the probe pulse will sample the coherences created by the pump pulse. As such, it is not accurate to use the rate equations to describe the pump/probe interaction.

For this reason, we have developed a nonperturbative model that is based on semiclassical theory. It combines the time-dependent density matrix equations with Maxwell's equations to describe the propagation of the pump and probe pulses. Our goal is to discover how well the rate equation model approximates the pump/probe interaction, when the model applies, or to find a similarly simple expression. This more exact model can also be used to define the limits of applicability for the rate equation expressions and then to explore other sensing possibilities offered by departures from the rate equation limits.

Density matrix models are commonly used to describe short-pulse spectroscopic interactions (see, for example, Refs. 6 and 7). The model described here is based on the development presented by Icsevgi and Lamb.[7] It combines three formalisms to self-consistently describe pulse propagation. First, the density matrix formalism of quantum mechanics describes the microscopic response of resonant and near-resonant atoms immersed in the laser field. Second, statistical physics describes how the individual atomic responses add up

to produce a net induced polarization on the macroscopic level. This statistical averaging explicitly accounts for Doppler broadening of the resonance. Last, from classical electrodynamics, we obtain the one-dimensional wave equation that describes the propagation of the laser pulse. Each of these topics will be discussed in three sections to follow. Prior to that, we will set the stage for those sections by introducing the formalism used to represent the laser pulses.

Pulse Representation

The pump and probe pulses will be described as plane waves traveling in the $\hat{e}_z$ direction with a linear electric field polarization in the $\hat{e}_x$ direction. The model described here, therefore, does not assume the crossed-beam geometry shown in Fig. 1 but instead a collinear geometry. The electric field of a pulse can be expressed as the product of a slowly varying envelope function and a rapidly varying phase, both of which are functions of the spatial coordinate z and the time t, with the complex conjugate (c.c.):

$$\boldsymbol{E}(z,t) = \hat{\boldsymbol{e}}_z \varepsilon(z,t)(\exp\{-i[\omega_0 t - k_0 z + \varphi(z,t)]\} + \text{c.c.}) \quad (2)$$

Both the angular frequency ω_0 and the propagation constant k_0 are considered constants, whereas the slowly varying phase term $\varphi(z,t)$ allows for dispersive effects. With no loss of generality, $\varphi(z,t)$ can be incorporated into the envelope function, resulting in a complex envelope function with real and imaginary components ε^R and ε^I:

$$\boldsymbol{E}(z,t) = \hat{\boldsymbol{e}}_z\{\tilde{\varepsilon}(z,t)\exp[-i(\omega_0 t - k_0 z)] + \text{c.c.}\} \quad (3)$$

This transformation allows us to describe the propagation of a pulse solely in terms of the propagation of a complex envelope because the rapidly varying phase term does not change form. We describe the net induced polarization of the sample in an analogous way:

$$\boldsymbol{P}(z,t) = \hat{\boldsymbol{e}}_z\{\tilde{p}(z,t)\exp[-i(\omega_0 t - k_0 z)] + \text{c.c.}\} \quad (4)$$

Because the pump and probe pulses are produced from the same laser by using a beam splitter, their envelope functions have the same functional form with the same initial phase, but they can have different magnitudes. Also, when describing both pulses in the same coordinate system, a spatial transformation must be applied to the probe pulse. This is because the pump and probe pulses travel through different pathlengths on their way to the interaction volume. If the probe pathlength is a distance Δz longer than that of the pump, the necessary spatial transform is $z \to z + \Delta z$. Because the beams are collinear through the interaction volume, the superposition principle can be used to describe the total field due to both pulses. Assuming that both pulses have the same electric field polarization, the total electric field is equal to the sum of the two fields, and the vector notation can be dropped. If the pump and probe pulses are each expressed as in Eq. (2), the total electric field takes the form of Eq. (3), where the real and imaginary parts of the total envelope function are given by the following expressions:

$$\varepsilon^R(z,t) = \varepsilon_1(z,t)\cos\varphi + \varepsilon_2(z+\Delta z,t) \times [\cos\varphi\cos k_0\Delta z + \sin\varphi\sin k_0\Delta z] \quad (5a)$$

$$\varepsilon^I(z,t) = -\varepsilon_1(z,t)\sin\varphi + \varepsilon_2(z+\Delta z,t) \times [\cos\varphi\sin k_0\Delta z - \sin\varphi\cos k_0\Delta z] \quad (5b)$$

An example of an envelope function used to describe a pump and a probe pulse in this manner is shown subsequently.

Density Matrix Equations

We use the density matrix formalism to describe the response of resonant or near-resonant atoms to the electric field of a laser pulse. Definition of the density matrix, discussion of its properties, and the derivations of the density matrix equations are found in most graduate quantum mechanics textbooks.[8] Additionally, we have found several books that contain useful introductions to this formalism, with particular emphasis on laser–matter interaction.[9–11]

For the purposes of this study, we will model a resonant atom or molecule as a closed two-level system. This simplification can be justified in cases where the resonance is isolated and where transfer rates between the resonant energy levels and other energy levels are negligible on the timescales considered by the model. The two-level system that will be considered is shown in Fig. 2. The combined spontaneous emission and collisional de-excitation rates are given by Γ_{21}. The collisional dephasing rate γ_{21} accounts for collisional broadening. Collisional excitation rates are considered negligible.

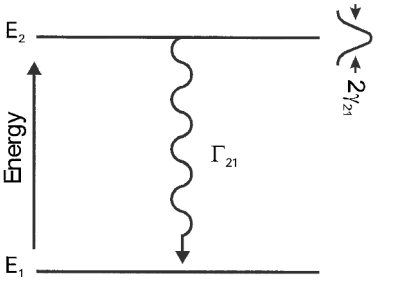

Fig. 2 Energy-level diagram for a closed two-level system, collisional/radiative deexcitation (with a rate Γ_{21}), and collisional broadening (characterized by the coherence dephasing rate γ_{21}).

The density matrix ρ for an atom contains all necessary information about this quantum system. For a two-level atom, the diagonal elements ρ_{11} and ρ_{22} are the probabilities that the atom is in state 1 or 2, respectively. For a closed two-level system, the trace of the density matrix must be equal to one inasmuch as the atom must be in one state or the other. The off-diagonal elements are the coherences between the states with the property that $\rho_{21} = \rho_{12}^*$.

When a resonant electric field is applied to an atom, the interaction Hamiltonian $\boldsymbol{V}$ is introduced into the Schrödinger equation. In the electric dipole approximation, the off-diagonal elements of the interaction Hamiltonian are given by

$$V_{21}(z,t) = -\mu_{21}E(z,t), \qquad V_{12}(z,t) = -\mu_{12}E(z,t) \quad (6)$$

In general, the off-diagonal elements are c.c. However, the dipole matrix elements μ_{12} and μ_{21} can be made purely real and equal, with no loss of generality, if the basis vectors describing the energy eigenstates 1 and 2 are judiciously chosen.

The density matrix equations are a set of coupled differential equations that describe the time evolution of the density matrix elements in response to an interaction Hamiltonian. With the relaxation rates defined earlier, the density matrix equations for a two-level system are given by[10]

$$\frac{\partial}{\partial t}\rho_{11} = \Gamma_{21}\rho_{22} + \frac{i}{\hbar}(V_{21}\rho_{12} - \rho_{21}V_{12}) \quad (7a)$$

$$\frac{\partial}{\partial t}\rho_{21} = -(i\omega_{21} + \gamma_{21})\rho_{21} + \frac{i}{\hbar}V_{21}(\rho_{22} - \rho_{11}) \quad (7b)$$

When the laser electric field is applied, the system responds at the optical frequency ω_0. As such, it stands to reason that the coherence can be written in terms of the product of a slowly varying complex envelope and the same rapidly varying phase term, as in Eq. (3):

$$\rho_{21} = \tilde{\sigma}_{21}\exp[-i(\omega_0 t - k_0 z)] \quad (8)$$

The envelope function for the coherence has real and imaginary parts σ_{21}^R and σ_{21}^I, respectively.

When the interaction Hamiltonian is expressed explicitly and Eq. (8) is substituted into the differential equations (7a) and (7b), the following two equations result:

$$\frac{\partial}{\partial t}\rho_{11} = \Gamma_{21}\rho_{22} + \frac{i\mu_{21}}{\hbar}(-\tilde{\varepsilon}\tilde{\sigma}_{21}^* + \tilde{\varepsilon}^*\tilde{\sigma}_{21} + \{\tilde{\varepsilon}\tilde{\sigma}_{21}\exp[-2i(\omega_0 t - k_0 z)] - \text{c.c.}\}) \quad (9a)$$

$$\frac{\partial}{\partial t}\tilde{\sigma}_{21} = -[i(\omega_{21} - \omega_0) + \gamma_{21}]\sigma_{21} - \frac{i\mu_{21}}{\hbar}(\rho_{22} - \rho_{11})\{\tilde{\varepsilon} + \tilde{\varepsilon}^*\exp[2i(\omega_0 t - k_0 z)]\} \quad (9b)$$

Equations (9) have terms that are slowly varying and terms that oscillate at twice the optical frequency. In the rotating wave approximation, the rapidly varying terms are neglected. Furthermore, these equations can be expressed in terms of the complex and real parts of the envelope functions for the electric field and for the coherences. This results in three real equations:

$$\frac{\partial}{\partial t}\rho_{11} = \Gamma_{21}(1-\rho_{11}) + \frac{2\mu_{21}}{\hbar}\left(\varepsilon^I\sigma_{21}^R - \varepsilon^R\sigma_{21}^I\right) \tag{10a}$$

$$\frac{\partial}{\partial t}\sigma_{21}^R = -\gamma_{21}\sigma_{21}^R + (\omega_{21}-\omega_0)\sigma_{21}^I + \frac{\mu_{21}}{\hbar}\varepsilon^I(1-2\rho_{11}) \tag{10b}$$

$$\frac{\partial}{\partial t}\sigma_{21}^I = -\gamma_{21}\sigma_{21}^I - (\omega_{21}-\omega_0)\sigma_{21}^R - \frac{\mu_{21}}{\hbar}\varepsilon^R(1-2\rho_{11}) \tag{10c}$$

Given an initial electric field envelope function, Eqs. (10) can be directly integrated to produce the time evolution of the coherence at a position z. The coherence is then used to calculate the atomic response, given by the expectation value of the atomic dipole moment. Using the formalism of quantum mechanics, the expectation value of any operator is given by the trace of the matrix resulting from the density matrix acting on the operator. For the dipole moment operator, which has nonzero elements only off diagonal, the expectation value is simply

$$\langle\mu\rangle = \rho_{12}\mu_{21} + \rho_{21}\mu_{12} = \mu_{21}\{\tilde{\sigma}_{21}\exp[-i(\omega_0 t - k_0 z)] + \text{c.c.}\} \tag{11}$$

Statistical Averaging

The net induced polarization is a macroscopic property that results from the sum of the microscopic responses of individual atoms, given by Eq. (11). The macroscopic polarization in a volume V is the volume average of the atomic dipole moments of all M atoms in V:

$$P(z,t) = \frac{1}{V}\sum_{i=1}^{M}\langle\mu\rangle_i \tag{12}$$

The atomic dipole moments in this problem can be parameterized by the atomic velocity component u along the optical axis $\hat{\boldsymbol{e}}_z$. Atoms traveling with different velocities along that axis will respond to the laser excitation at optical frequencies that are Doppler shifted. With this in mind, we introduce a more explicit notation that emphasizes this parameterization. A partial polarization $P(z,t;u)$ is defined as the time-dependent expectation value of the dipole moment of an atom at position z with a velocity component u:

$$P(z,t;u) = \langle\mu(z,t;u)\rangle \tag{13}$$

The summation in Eq. (12) is treated in statistical physics by introduction of the velocity distribution function. For this analysis, we consider a steady-state and spatially uniform Maxwellian velocity distribution, which is only a function of the velocity component u. In this case, the probability that an atom has a velocity component u in the interval $[u, u+\mathrm{d}u]$ is given by

$$f(u)\,\mathrm{d}u = \left(\frac{m}{2\pi k_B T}\right)^{\frac{1}{2}}\exp\left(-\frac{mu^2}{2k_B T}\right)\mathrm{d}u \tag{14}$$

Using this distribution function, Eq. (12) becomes the following integral:

$$P(z,t) = N_{\text{tot}}\int_{-\infty}^{+\infty}P(z,t;u)f(u)\,\mathrm{d}u \tag{15}$$

The partial polarization can be written in terms of the coherence envelope function. In the notation of Eq. (4), the envelope function for the net polarization is

$$\tilde{p}(z,t) = N_{\text{tot}}\mu_{21}\int_{-\infty}^{+\infty}\tilde{\sigma}_{21}(z,t;u)f(u)\,\mathrm{d}u \tag{16}$$

One-Dimensional Wave Equation

The one-dimensional wave equation is derived from Maxwell's equations, and it has the following form in SI units (to switch to Gaussian units, simply replace $1/\varepsilon_0$ with 4π):

$$\left[\frac{\partial^2}{\partial z^2} - \frac{1}{c^2}\frac{\partial^2}{\partial t^2}\right]E(z,t) = \frac{1}{\varepsilon_0 c^2}\frac{\partial^2}{\partial t^2}P(z,t) \tag{17}$$

It is desirable to reduce the second-order wave equation to a first-order differential equation. This reduction is possible using an important approximation and a small bit of algebra. First, Eqs. (3) and (4) are substituted into the wave equation. Next, invoking the slowly varying envelope approximation, second-order derivatives of the slowly varying functions $\varepsilon(z,t)$ and $p(z,t)$ are neglected. Furthermore, time derivatives of $p(z,t)$ can also be ignored with respect to the other terms in the equation. Finally, writing the wave equation in terms of the real and imaginary parts of the envelope functions, the following two real differential equations result from grouping terms that are in phase and in quadrature with the optical phase:

$$\left[\frac{\partial}{\partial z} + \frac{1}{c}\frac{\partial}{\partial t}\right]\varepsilon^R(z,t) = -\frac{k_0}{2\varepsilon_0}p^I(z,t) \tag{18a}$$

$$\left[\frac{\partial}{\partial z} + \frac{1}{c}\frac{\partial}{\partial t}\right]\varepsilon^I(z,t) = \frac{k_0}{2\varepsilon_0}p^R(z,t) \tag{18b}$$

A further simplification results by invoking the retarded time transformation $t \to \tau = t - z/c$. This change of variables transforms the wave equations from partial differential equations to two ordinary differential equations that can be directly numerically integrated:

$$\frac{\partial}{\partial z}\varepsilon^R(z,\tau) = -\frac{k_0}{2\varepsilon_0}p^I(z,\tau) \tag{19a}$$

$$\frac{\partial}{\partial z}\varepsilon^I(z,\tau) = \frac{k_0}{2\varepsilon_0}p^R(z,\tau) \tag{19b}$$

Pump/Probe Model

The five differential equations describing this system are given in Eqs. (10) and (19). These equations are repeated using explicit notation for the dependencies of the variables:

$$\frac{\partial}{\partial\tau}\rho_{11}(z,\tau;u) = \Gamma_{21}[1-\rho_{11}(z,\tau;u)] + \frac{2\mu_{21}}{\hbar}\left[\varepsilon^I(z,\tau)\sigma_{21}^R(z,\tau;u) - \varepsilon^R(z,\tau)\sigma_{21}^I(z,\tau;u)\right] \tag{20a}$$

$$\frac{\partial}{\partial\tau}\sigma_{21}^R(z,\tau;u) = -\gamma_{21}\sigma_{21}^R(z,\tau;u) + [\omega_{21}-\omega(u)]\sigma_{21}^I(z,\tau;u) + \frac{\mu_{21}}{\hbar}\varepsilon^I(z,\tau)[1-2\rho_{11}(z,\tau;u)] \tag{20b}$$

$$\frac{\partial}{\partial\tau}\sigma_{21}^I(z,\tau;u) = -\gamma_{21}\sigma_{21}^I(z,\tau;u) - [\omega_{21}-\omega(u)]\sigma_{21}^R(z,\tau;u) - \frac{\mu_{21}}{\hbar}\varepsilon^R(z,\tau)[1-2\rho_{11}(z,\tau;u)] \tag{20c}$$

$$\frac{\partial}{\partial z}\varepsilon^R(z,\tau) = -\frac{k_0}{2\varepsilon_0}p^I(z,\tau) \tag{20d}$$

$$\frac{\partial}{\partial z}\varepsilon^I(z,\tau) = \frac{k_0}{2\varepsilon_0}p^R(z,\tau) \tag{20e}$$

The first three differential equations describe the time evolution of the density matrix at a particular spatial location for an atom with a particular velocity component. The atoms addressed by these equations will see a Doppler-shifted laser frequency, and as such, the apparent laser frequency ω is shown to have velocity dependence. The Doppler-shifted frequency is

$$\omega(u) = \omega_0 - k_0 u \tag{21}$$

The last two differential equations relate the spatial gradient of the electric field to the induced polarization. The induced polarization envelope functions are directly related to the coherence envelope functions as follows:

$$p^R(z,\tau) = N_{\text{tot}}\mu_{21}\left(\frac{m}{2\pi k_B T}\right)^{\frac{1}{2}} \times \int_{-\infty}^{+\infty} \sigma_{21}^R(z,\tau;u)\exp\left(-\frac{mu^2}{2k_B T}\right)\mathrm{d}u \tag{22a}$$

$$p^I(z,\tau) = N_{\text{tot}}\mu_{21}\left(\frac{m}{2\pi k_B T}\right)^{\frac{1}{2}} \times \int_{-\infty}^{+\infty} \sigma_{21}^I(z,\tau;u)\exp\left(-\frac{mu^2}{2k_B T}\right)\mathrm{d}u \tag{22b}$$

These equations are solved numerically across a spatial and temporal grid, to give populations in the upper and lower quantum states together with the atomic coherences. These are then used to provide the macroscopic polarization as a function of space and time. The input field envelope is defined such that it includes both the pump and probe pulses, and the model calculates the attenuation/gain of the envelope as the pulses propagate through the sample volume. The pump pulse, thus, prepares a series of states that are then sensed by the probe pulse as it propagates along the same centerline. The modulation depth can then be inferred from the change in irradiance of the probe pulse.

Integration of the density matrix equations was performed using a Burlirsch–Stoer extrapolation technique.[12] When required, the integrals in Eqs. (22) are solved using Gauss–Hermite quadrature, with the necessary routines also coming from Ref. 12. Equations (20d) and (20e) are solved using a simple one-step predictor–corrector method, which is started with a single forward Euler step at $z = 0$. A detailed description of the numerical scheme is provided in Ref. 3.

We confirmed that the time integration of the density matrix equations was correct by comparing simulation results to steady-state analytical solutions. To do this, a constant electric field was turned on at time zero, and the integrator marched forward in time until the population and coherences reached steady-state values. These numerical results were then compared to the analytical expressions. Using a range of very weak to strongly saturating electric fields, both collision-free and strongly quenching environments, and a range of laser wavelengths covering five times the full width at half maximum (FWHM) of the absorption linewidth, we achieved excellent agreement with the analytical solutions. In all cases, the real and imaginary susceptibilities were within $\pm 0.1\%$ of the analytical values, and the resulting excited state population was within $\pm 0.01\%$.

Performance of the pulse energy integration, used to calculate the integrated attenuation at each z position, was evaluated by invoking an energy balance. The number of excited atoms was calculated on each position interval, and this was compared to the number of photons absorbed on the same interval. Conservation of energy dictates that these two numbers are the same in the absence of relaxation phenomena. Over a wide range of pulse energies, these two agreed to within a fraction of a percent.

A grid refinement study was employed to investigate numerical accuracy associated with the calculation of modulation depth. It was found that the simulation results converged with a spread of approximately $\pm 2\%$ as the position grid spacing was successively reduced. We reduced the spacing to the point that truncation errors started to prevail and, as such, identified suitable limits for the spatial grid.

Density Matrix Model Results

We now present some model results for pulse propagation in pump/probe experiments using potassium. We are focusing on potassium because we wish to perform detailed experimental validation of model results. Potassium has several advantages that make it ideal for this characterization. It has two well-known, strong ground-state transitions in the fundamental tuning range of Ti:sapphire. These lines are sufficiently spaced that a two-level interaction is appropriate. Therefore, we can be certain that our model accurately describes the physical interaction. All subsequent simulations use 2-ps pulses and parameters typical of the experimental conditions that follow.

Experimental Parameters

The experiments will employ the Spectra-Physics regeneratively mode-locked Ti:sapphire laser system described earlier. The beam diameter is approximately 100 μm at the sample volume. Assuming a sech^2 intensity profile and 1.85-W average power, the electric field magnitude at the sample is approximately 1.5×10^7 V/m for the 2-ps pulses. The transform-limited spectral FWHM of a 2-ps pulse is $\Delta\omega_{2\text{ps}} = 0.99\ \text{ps}^{-1}$.

The laser will be tuned to the $4^2S_{1/2}$–$4^2P_{1/2}$ transition of atomic potassium at 769.9 nm. Although both the ground and excited states are twofold degenerate, we can still treat the resonance as a two-level system because the laser pulses are linearly polarized.[13] In this case, the two degenerate ground states are coupled to the two degenerate excited states through two equivalent π transitions. In this configuration, there can be no coherences formed between the degenerate states in either the ground or excited states. The spontaneous emission coefficient for the $4^2S_{1/2}$–$4^2P_{1/2}$ transition[14] is approximately $0.382 \times 10^8\ \text{s}^{-1}$. This value corresponds to a dipole moment of 2.5×10^{-29} C · m. Fiechtner and Linne[2] probed the $4^2S_{1/2}$–$4^2P_{3/2}$ transition (766.5 nm) in prior pump/probe experiments. For the conditions of their experiments, it was determined to avoid saturation; the pump and probe beam powers had to be kept below 4 mW (49 pJ per pulse) and 5 mW (61 pJ/pulse), respectively.[15]

Two sources of potassium will be used in experiments. A low-pressure atomic vapor cell will be used initially to provide well-characterized number densities. This cell has four windows arranged in a tee, so that we can perform spectrally resolved absorption measurements simultaneously with pump/probe determinations. A Winefordner-style aspirating burner can also be used to seed potassium into an atmospheric methane/air flame. This device was used to provide parameters for the model to simulate a combustion diagnostic more closely. We assume an equilibrium temperature of approximately 2000 K, which corresponds to a FWHM of the potassium velocity distribution of 922 m/s. The corresponding Doppler broadening of the atomic line is $\Delta\omega_{\text{Doppler}} = 7.5 \times 10^{-3}\ \text{ps}^{-1}$.

For simulations involving 2-ps pulses, the temporal discretization is typically set to 0.04 ps so that 50 grid points span the intensity FWHM. The spatial discretization is chosen so that the difference between the predictor and corrector steps is kept within a 0.2% tolerance. When Doppler broadening is explicitly included in the simulations, 19 velocity groups are used in the integration.

Initial Conditions

We assume that when unperturbed, all atoms are in the ground state. Furthermore, the coherences must be zero when no coherent excitation is present. We further assume that the mode-locked laser pulses are described by hyperbolic secant envelope functions. The envelope function for the pump has a magnitude ε_1, and it peaks at $\tau = \tau_1$. The probe envelope has a magnitude ε_2, and it peaks at $\tau = \tau_2$. The pulses are spatially separated by $\Delta z = c(\tau_2 - \tau_1)$. Each pulse has the same intensity FWHM, which is denoted $\Delta\tau_{\text{FWHM}}$. Using Eq. (5), the electric field envelope is specified at $z = 0$ by the following two functions:

$$\varepsilon^R(0,\tau) = \varepsilon_1 \operatorname{sech}\left[\frac{-2\ln(\sqrt{2}-1)}{\Delta\tau_{\text{FWHM}}}(\tau-\tau_1)\right]\cos\varphi + \varepsilon_2 \operatorname{sech}\left[\frac{-2\ln(\sqrt{2}-1)}{\Delta\tau_{\text{FWHM}}}(\tau-\tau_2)\right] \times [\cos\varphi\cos k_0\Delta z + \sin\varphi\sin k_0\Delta z] \tag{23a}$$

$$\varepsilon^I(0,\tau) = -\varepsilon_1 \operatorname{sech}\left[\frac{-2\ln(\sqrt{2}-1)}{\Delta\tau_{\text{FWHM}}}(\tau-\tau_1)\right]\sin\varphi + \varepsilon_2 \operatorname{sech}\left[\frac{-2\ln(\sqrt{2}-1)}{\Delta\tau_{\text{FWHM}}}(\tau-\tau_2)\right] \times [\cos\varphi\sin k_0\Delta z - \sin\varphi\cos k_0\Delta z] \tag{23b}$$

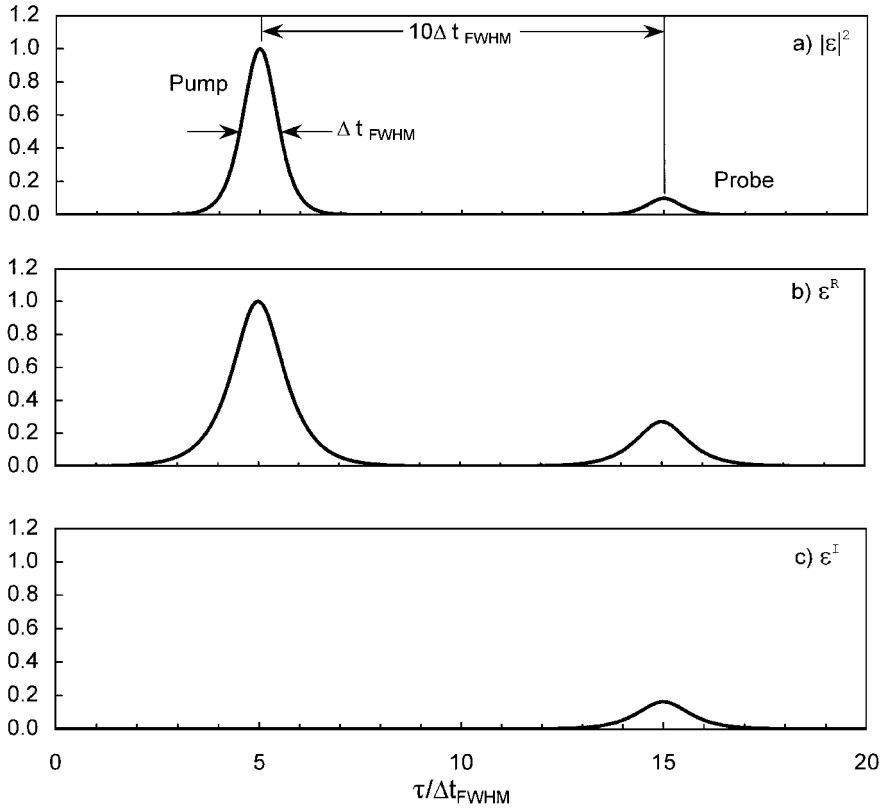

Fig. 3 Example of the electric field envelope for $z = 0$: a) square of the magnitude of the envelope function, b) real part of the complex envelope function, and c) imaginary part of the envelope function.

Figure 3a shows the modulus squared for a pump/probe envelope. In this example, the phase is set so that the pump envelope is purely real at $z = 0$ [$\varphi(0, \tau) = 0$ in Eq. (2)]. The probe irradiance is 10% of the pump irradiance. The peak of the pump pulse occurs at $\tau_1 = 5\Delta\tau_{\text{FWHM}}$, and the probe pulse peaks at $\tau_2 = \tau_1 + 10\Delta\tau_{\text{FWHM}}$.

For the numerical integration, it is important to truncate the envelope functions, so that the laser electric field is always zero for $\tau \leq 0$. A further restriction is placed on the functions to distinctly separate the pump and probe pulses. This is accomplished by setting the electric field for each pulse to zero for $|\tau - \tau_{\text{peak}}| > 4.5\Delta\tau_{\text{FWHM}}$. We have evaluated this approach three ways: by truncating with a step, by truncating with a linear ramp, and by allowing one pulse to propagate much further without truncation and without the second pulse. No matter how the tail of the pump pulse is dealt with, the coherences created by the pulse itself impose their lifetime on the populations. Calculations indicate that the second probe pulse encounters populations that are identical, no matter how the pump pulse is truncated.

Figures 3b and 3c show the real and imaginary parts of the envelope function as determined from Eq. (23). When considered independently, the pump and probe pulses were taken to be purely real. However, when the envelope function for both pulses is calculated, the imaginary part is nonzero due to the phase $k_0\Delta z$ introduced by the pump–probe delay.

Note that very slight changes in Δz, on the order of a fraction of an optical wavelength, can dramatically change the envelope function. For example, if Δz is set so that the envelope is purely real, coherences due to the pump pulse are exactly in phase with the probe pulse. If Δz is then shifted one-half of an optical wavelength, the pump and probe are exactly out of phase. Shifts of this magnitude will most definitely occur in an experiment. To calculate modulation depth, therefore, we average the modulation in probe energy over all of the possible phase shifts.

Doppler Effects

The model includes Doppler effects by averaging atomic responses over a Maxwellian distribution. However, for potassium, under atmospheric flame conditions, Doppler broadening is negligible with respect to the spectral bandwidth of a 2-ps pulse. At 2000 K, the Doppler width for potassium is two orders of magnitude smaller than the laser spectral bandwidth. Therefore, atomic responses vary little for velocity groups within the Maxwellian distribution, and the average atomic response turns out to be the response that is calculated for stationary atoms. Therefore, the remaining simulations do not carry out the statistical average explicitly.

Single-Pulse Propagation

The circles in Fig. 4 indicate actual simulation results and show the excited state population at $\tau = \tau_{\text{peak}} + 4.5\Delta\tau_{\text{FWHM}}$ extracted from the density matrix model (DM) that results after a single-pulse interaction. Note that connecting lines are only included to aid visualization and are not simulation data. Also shown in Fig. 4 are two rate equation (RE) results. The curve labeled linear RE uses the same linearization that appears in the development of Eq. (1), that stimulated absorption of the pump pulse is included but stimulated emission is not. The curve labeled simply RE includes both stimulated absorption and emission by the pump pulse. Both RE results assume a temporal top-hat profile. For this specific simulation, collisions were neglected by appropriately setting the excited state and coherence lifetimes. As such, relaxation effects were negligible. This allowed a fair comparison between the simulation results and the RE results, which included no relaxation terms.

Initially, the DM excited state population scales linearly with pulse energy, consistent with the REs. For pulse energies less than 60 pJ (5-mW cw), the error introduced by using the linear RE is less than 5.6%, and for pulse energies less than 120 pJ (10-mW cw), the error is less than 11%. In this weak pulse limit, the linear RE always overpredicts the population. These errors become even larger when collisional effects are included in the DM model. Furthermore, the linearized RE pump/probe model [Eq. (1)] assumes that this population is constant throughout the sample volume. In fact, the pump pulse is attenuated and, therefore, even smaller populations result as the pulse propagates through the sample. As such, the approximations used to describe the pump interaction in the linearized RE pump/probe model always overpredict the excited state population.

The RE model predicts steady-state saturation when stimulated emission and stimulated absorption are balanced. This limit is

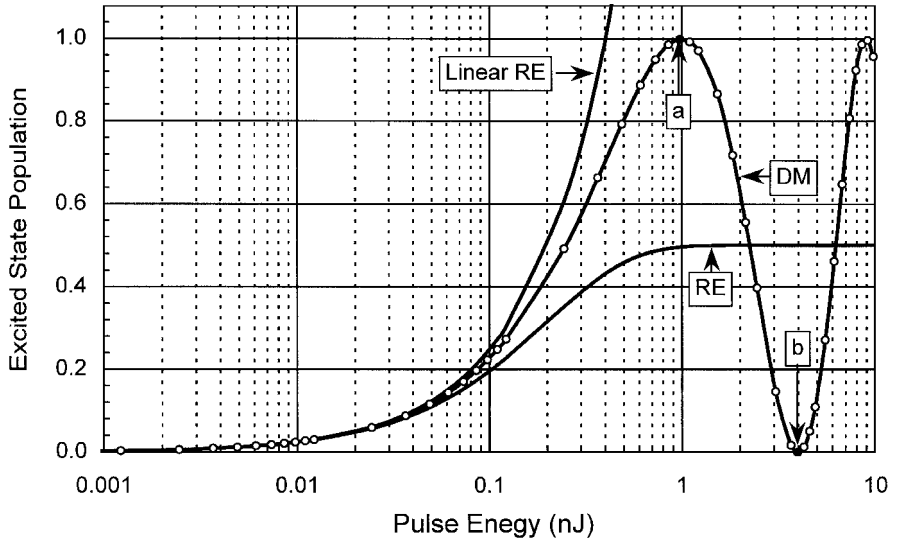

Fig. 4 Excited state population of potassium vs pulse energy.

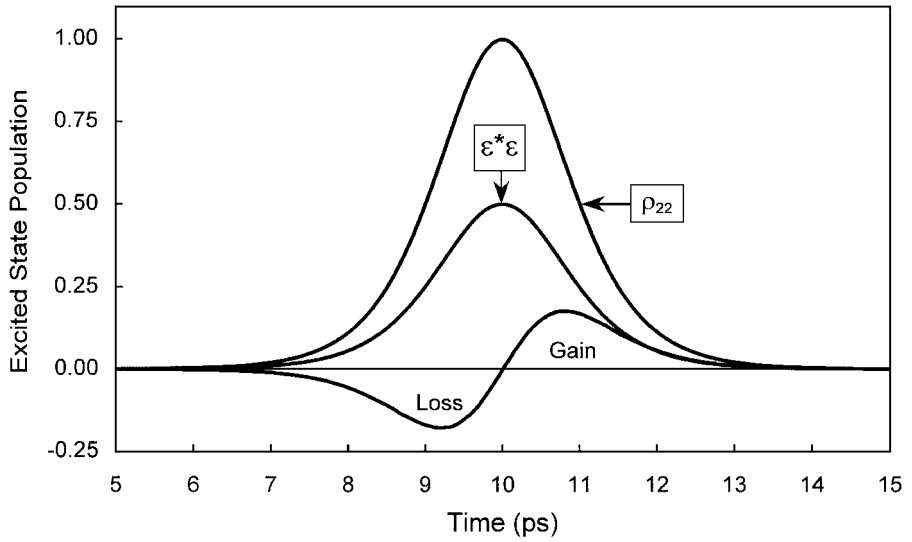

Fig. 5 Time history of the pulse irradiance $\varepsilon^*\varepsilon$, the excited state population ρ_{22}, and the pulse gain, shown for a 4-nJ pulse after propagating through 2 mm of potassium at 10^{11} cm^{-3}.

approached as the laser irradiance is increased, and in this limit, a two-level system has equal population in each state. However, the DM-based model shows that as the pulse energy increases to 1 nJ, the excited state population does not saturate at a value of 0.5. Instead, as indicated by point a in Fig. 4, almost all of the population is in the excited state. If the pulse energy is increased still further, the population is stimulated back toward the ground state. At point b, at 4 nJ (325-mW cw), almost all of the population is back in the ground state. The excited state population and the laser attenuation for a pulse with energy at point b of Fig. 4 are both plotted as a function of time in Fig. 5. Because little collisional relaxation occurs on these short timescales, conservation of energy dictates that that this pulse sees very little integrated attenuation. This is shown in Fig. 5, where the first half of the pulse is attenuated and the second half experiences gain. The time-integrated gain is approximately zero. This behavior has been extensively studied and is termed self-induced transparency. McCall and Hahn[16] wrote the definitive paper on this subject in 1969.

An interesting phenomenon occurs for pulses with energy greater than that corresponding to point a in Fig. 4. In these cases, the population flops back and forth during the pulse. If the electric field of the pulse is constant, these oscillations occur at a fixed frequency, the Rabi frequency Ω_{Rabi}. In general, the Rabi frequency is time dependent and is related to the electric field envelope by

$$\Omega_{\text{Rabi}} = \frac{\mu_{21}\varepsilon(t)}{\hbar} \tag{24}$$

Figure 6 shows the Rabi oscillation corresponding to the maximum pulse we can produce with our unamplified Ti:sapphire laser. The pulse energy is 22.6 nJ (1.85-W cw). The net result is an excited state population of 0.86, the same result produced by 0.6-, 1.5-, 7.5-, and 10.4-nJ pulses. Although this phenomenon is interesting, for our purposes it is undesirable to operate in this regime. The state of the atomic population following a pulse that induces Rabi oscillations is highly sensitive to pulse shape, height, and duration. Laser fluctuations can result in very unpredictable behavior, which makes correct characterization of the pump/probe experiment impossible.

Pump/Probe Spectroscopy: Comparison Between the RE and DM Formalisms

The earlier results, shown in Fig. 4, suggest that the potassium pump/probe signal will most likely be linear when pulse energies are less than 0.1 nJ. The models were exercised, therefore, in this region. A probe pulse energy of 1.2 pJ (100-μW cw) was used in the following cases, and we varied the pump energies from 6.1 to 122 pJ. We have simulation results for these pump and probe energies, while varying the product of the total number density and the interaction length ($N_{\text{tot}}l$) from 2×10^9 to 2×10^{12} mm cm^{-3}. Currently, truncation errors prevent us from obtaining results with $N_{\text{tot}}l < 2 \times 10^9$ mm cm^{-3}. This issue will be addressed in a future version of the code.

Figure 7 compares modulation depth predicted by the linearized RE model (circles) and the DM simulation (lines) for five pump

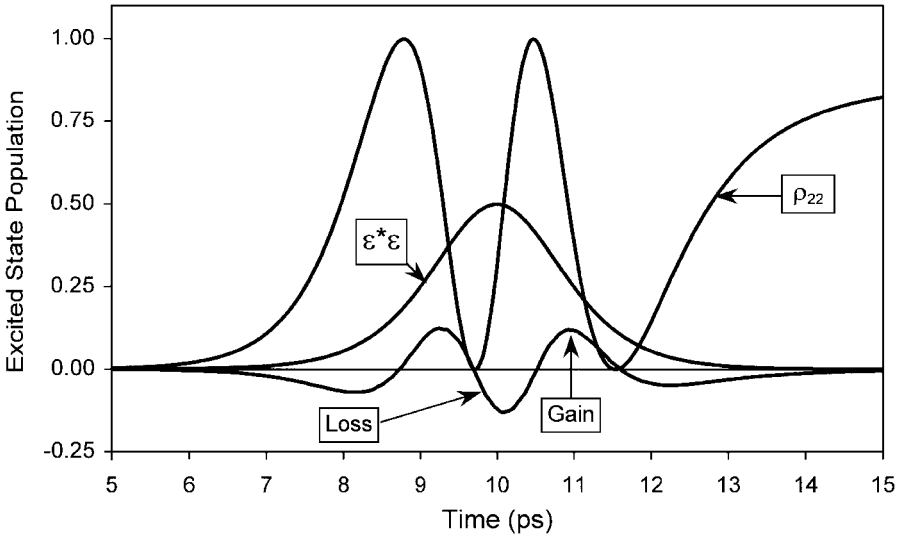

Fig. 6 Time history of the pulse irradiance $\varepsilon^*\varepsilon$, the excited state population ρ_{22}, and the pulse gain, for a 22.6-nJ pulse after propagating through 2 mm of potassium at 10^{11} cm^{-3}.

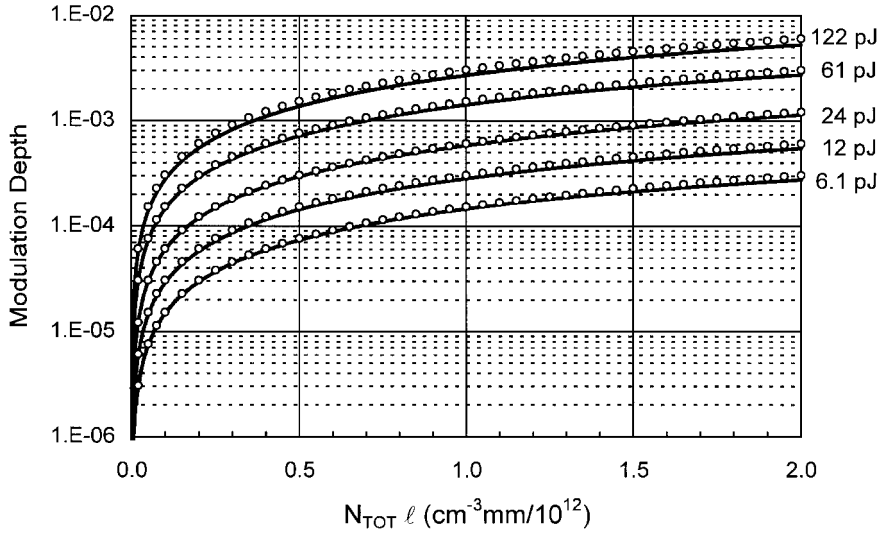

Fig. 7 Predicted modulation depth vs $N_{tot}l$, for various pump pulse energies.

pulse energies. The pump energies are noted on the right-hand side of the graph. To give the two models an equal footing, collisional effects were neglected in the DM calculations, so that relaxation phenomena are negligible over the pump/probe interaction. One can observe immediately that the agreement between the two is encouraging.

For pump energies less than or equal to 61 pJ (5-mW cw), the two models agree to within 10%. As the pump energy is increased to obtain larger signals, however, the error gets larger and is on the order of 15% for a 122-pJ (10-mW) pump. Furthermore, the error increases with $N_{tot}l$. This effect is due to both pump attenuation and coherence effects. The linear RE model addresses neither of these phenomena.

When collisional effects characteristic of the flame environment are used, the RE model becomes a slightly worse estimate. The DM simulation was used to calculate the modulation depth for relaxation times of 100 ps, 200 ps, 1 ns, and for the collision-free case. The modulation depth for a 24-pJ pump and a 1.2-pJ probe are shown for these relaxation times in the top half of Fig. 8. The RE-based prediction is shown as circles. The errors between the DM and the RE results are plotted for the four values of relaxation times in the bottom half of the graph. There is essentially no difference between the results for the relaxation time of 1-ns and collision-free case. Furthermore, there is only a 5% difference between the modulation depth for the relaxation time equal to 100 ps and the modulation depth for the collision-free case. These simulations support our claim that this technique can be effectively used in collisional environments.

These results then set the limits within which RE expressions can be applied, while maintaining reasonable uncertainties. More exact DM models can certainly be applied to experimental measurements to improve accuracy, but the simplicity of the RE results is compelling. An outcome as simple as Eq. (1) is likely to have broader application than a numerical solution to the DM equations.

One could reasonably ask whether it might be possible to achieve even better agreement between the REs and the DM model. Three basic approximations are made in the RE model. The first is a temporal top-hat profile. The REs predict the same results with a top-hat profile as they do a sech^2 profile, consistent with the expectations of Fiechtner et al.[4] The second is an assumption that the interaction is optically thin, which removes spatial dependence (z axis) from the model. In this assumption, the pump pulse irradiance together with state populations following the pump pulse are both invariant with z. The DM equations predict spatially varying populations and pump pulse attenuation with z, in disagreement with the RE result. Finally, high pump pulse energy produces larger signals, but in this regime the pump pulse stimulates emission. This effect is also not accounted for in the RE model. Given these facts, it seems that the RE model could be made more accurate by including stimulated emission in the pump portion of the model and integrating the rate equations along z, thus allowing for spatial changes in the pump-prepared populations. Whereas this would make it impossible to apply a simple equation such as Eq. (1), integration of the REs along z is straightforward and should not impair application of

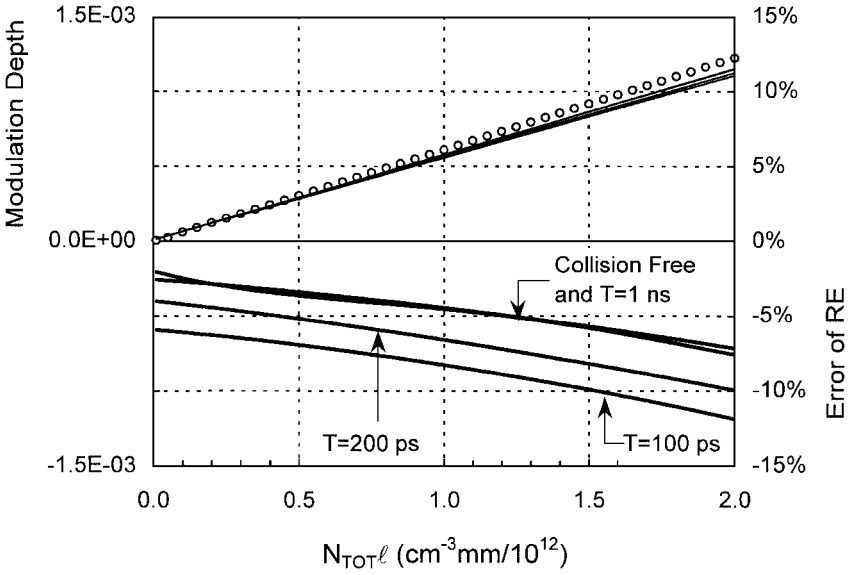

Fig. 8 Predicted modulation depth vs $N_{tot}l$ (upper set of curves) and errors between the linear RE and DM results (lower set of curves) for various relaxation times ($1/\Gamma_{21}$ and $1/\gamma_{21}$).

the diagnostic. These hypotheses will be tested as we examine both models during potassium-based experimentation.

Conclusions

This paper presents a basic discussion of the RE and DM models that we are currently developing to study pulse propagation in pump/probe experiments. The nonperturbative DM model does not use any simplifying assumptions with regard to pulse intensities and treats the atomic response with a quantum mechanically correct formalism. This model has been developed in an attempt to either validate the RE-based model or to identify a similar kind of relationship. Furthermore, the model can be used to maximize signal while staying within the experimental limits of applicability of this relationship.

Simulation results were presented to demonstrate qualitative behavior as a function of both pump pulse energy and total number density. Experimental parameters for a potassium pump/probe experiment were used, and the simulations demonstrated linear behavior in the weak interaction limit. Our results have indicated that if pump/probe experiments are conducted within well-defined limits to laser power and optical depth, the simple RE approach can be used with errors $\leq$15%. Suggestions are made for improvement of this result. A departure from linearity was observed as the interaction strength was increased. When the laser pulses are sufficiently strong to cause Rabi oscillations in the atomic populations, it is no longer possible to characterize the experiment with simple expressions.

The atomic response of a gaseous system to a resonant picosecond pulse is always a transient one, which cannot be represented by the RE formalism. However, we have shown that the integrated response for a two-level resonance is well represented by the REs for very weak interactions. As a rough rule of thumb, this condition is typically met when both the integrated absorption and the perturbed population are less than 1%.

In the future, we will perform detailed experiments in a potassium cell and an aspirating burner seeded with potassium to verify these findings. These experiments will include a line-of-sight atomic absorption measurement that will be used as the known concentration determination. Pump/probe modulation depths will be measured and used in various formulations of the RE model and in the DM model to verify our findings. The range of applicability for the REs and departures from RE behavior will also be explored.

Acknowledgments

This research has been supported by the National Science Foundation through Grants CTS-9411391, CTS-9711889, and DGE-9554559 and by the U.S. Air Force Wright Laboratories through Grant F33615-96-C-2632.

References

[1]Eckbreth, A. C., *Laser Diagnostics for Combustion, Temperature and Species*, 2nd ed., Gordon and Breach, Amsterdam, 1996.

[2]Fiechtner, G. J., and Linne, M. A., "Absolute Concentrations of Potassium by Picosecond Pump/Probe Absorption in Fluctuating, Atmospheric Flames," *Combustion Science and Technology*, Vol. 100, No. 1, 1994, pp. 11–27.

[3]Linne, M., Settersten, T., Gord, J., and Fiechtner, G., "Developments in Picosecond Pump/Probe Diagnostics," AIAA Paper 98-0306, Jan. 1998.

[4]Fiechtner, G. J., King, G. B., and Laurendeau, N. M., "Rate-Equation Model for Quantitative Concentration Measurements in Flames with Picosecond Pump-Probe Absorption Spectroscopy," *Applied Optics*, Vol. 34, No. 6, 1995, pp. 1108–1116.

[5]Heritage, J. P., "Picosecond Nonlinear Spectroscopy of Silver Microstructures and Surface Absorbates," *Advances in Laser Spectroscopy 2*, edited by B. A. Gartez and J. R. Lombardi, Wiley, New York, 1983, pp. 207–224.

[6]Melinger, J. S., Gandhi, S. R., Hariharan, A., Goswami, G., and Warren, W. S., "Adiabatic Population Transfer with Frequency-Swept Laser Pulses," *Journal of Chemical Physics*, Vol. 101, No. 8, 1994, pp. 6439–6454.

[7]Icsevgi, A., and Lamb, W. E., "Propagation of Light Pulses in a Laser Amplifier," *Physical Review*, Vol. 185, No. 2, 1969, pp. 517–545.

[8]Sakurai, J. J., *Modern Quantum Mechanics*, Addison–Wesley, New York, 1985, pp. 170–187.

[9]Lalanne, J. R., Ducasse, A., and Kielich, S., *Laser-Molecule Interaction: Laser Physics and Molecular Nonlinear Optics*, Wiley, New York, 1996, pp. 3–28.

[10]Boyd, R. W., *Nonlinear Optics*, Academic, San Diego, CA, 1992, pp. 116–123, 192–199.

[11]Verdeyen, J. T., *Laser Electronics*, 3rd ed., Prentice–Hall, Englewood Cliffs, NJ, 1995, pp. 627–639.

[12]Press, W. H., Teukolsky, S. A., Vetterling, W. T., and Flannery, B. P., *Numerical Recipes in C: The Art of Scientific Computing*, 2nd ed., Cambridge Univ. Press, New York, 1992, pp. 724–732.

[13]Allen, L., and Eberly, J. H., *Optical Resonance and Two-Level Atoms*, Dover, New York, 1987, pp. 117, 118.

[14]Wiese, W. L., Smith, M. W., and Glennon, B. M., *Atomic Transition Probabilities (Na through Ca—A Critical Data Compilation)*, National Standard Reference Ser., National Bureau of Standards 22, Vol. II, U.S. Government Printing Office, Washington, DC, 1966.

[15]Fiechtner, G. J., "Quantitative Concentration Measurements in Atmospheric-Pressure Flames by Picosecond Pump/Probe Absorption Spectroscopy," Ph.D. Dissertation, School of Mechanical Engineering, Purdue Univ., Lafayette, IN, April 1992.

[16]McCall, S. L., and Hahn, E. L., "Self-Induced Transparency," *Physical Review*, Vol. 183, No. 2, 1969, pp. 457–485.

R. P. Lucht
Associate Editor